Regular waves onto a truncated circular column: a comparison of experiments and simulations

L. Sun [a,*], J. Zang [a], L. Chen [a], R. Eatock Taylor [b], P. H. Taylor [b]

[a] *WEIR Research Unit, Department of Architecture and Civil Engineering, University of Bath, Bath BA2 7AY, UK*

[b] *Department of Engineering Science, University of Oxford, Parks Road, Oxford OX1 3PJ, UK*

ABSTRACT

Accurate prediction of hydrodynamic forces on offshore structures is critical for safe and cost effective design of fixed and floating offshore structures exposed to a harsh environment. In the present paper, nonlinear interactions between regular waves and a single surface-piercing truncated circular column have been investigated using a frequency domain potential flow solver (DIFFRACT) and a full CFD solver in OpenFOAM for direct comparisons. Both the predicted free surface elevation around the column and the total force acting on the column have been analysed and compared with experimental data from MOERI. The degree of non-linearity and the contribution of each harmonic to the free surface run-up and wave forces have been examined, and evaluations of the accuracy and computational efficiency of the potential flow solver and the full CFD solver are provided and compared in the paper. Also of note are the local forms of the scattered waves around the column in numerical simulations, which are consistent with the Type-1 and Type-2 patterns identified in physical experiments at Imperial College.

Keywords: potential flow; CFD; OpenFOAM; nonlinear surface elevation; nonlinear force; truncated circular column

1. Introduction

Safety is always a major concern in the design of offshore structures. Offshore structures are expected to have an acceptably low probability of failure so should survive most severe sea states. Sufficient air gap is required for all offshore oil and gas platforms to avoid wave impact on upper structures or equipment close to deck level. For floating structures, efforts have been made to minimize the wave induced motions to reduce fatigue damage to drill strings and risers. So wave-structure interaction is a key ingredient in the

* Corresponding author. Tel.: +44 (0) 1225 385206
Email addresses: l.sun@bath.ac.uk (L. Sun), j.zang@bath.ac.uk (J. Zang), lc499@bath.ac.uk (L. Chen), r.eatocktaylor@eng.ox.ac.uk (R. Eatock Taylor), paul.taylor@eng.ox.ac.uk (P. H. Taylor)

design of offshore structures. In contrast, for wave energy devices, energy is extracted from the device motions.

For interactions between waves and structures with simple geometries, analytical or semi-analytical solutions can be obtained [1, 2]. To analyse the interactions between waves and complex offshore structures, numerical simulations and model tests are needed. Software packages based on the first- and second-order potential flow theory have been available and widely applied in the offshore industry for many years [3, 4]. In frequency domain analysis, it is convenient and efficient to obtain response amplitude operators (RAOs) and quadratic transfer functions (QTFs) for free surface elevations and wave forces. However, contributions from components above second order may also produce some novel phenomena for large wave conditions. A good example is 'ringing' which has been observed in model tests and prototype experiments on surface-piercing columns such as those in tension-leg platforms (TLPs) and gravity-based structures (GBS). These may experience sudden bursts of highly amplified resonant vibrations during storms [5]. Fully nonlinear numerical wave tanks (NWT) based on potential flow theory have been developed to investigate nonlinear properties of wave-structure interactions [6-10].

Another factor relevant to the accuracy of predictions in numerical simulations is the possible importance of viscous effects. It is expected that potential flow solvers may generally over-predict local surface elevations in near-trapping problems [11]. It is also a great challenge for potential flow solvers to simulate the local nonlinear free surface motion correctly when wave breaking occurs. Full CFD solvers which can account for viscous effects as well as large distortions of the free surface motion may give more accurate predictions, although solutions can require considerable computational resources [12]. In recent years, the open-source CFD software package OpenFOAM has become increasingly popular for applications in coastal and offshore engineering [13-16]. Being open source, OpenFOAM offers researchers complete freedom to customize and extend its existing functionality.

The present work is focused on the assessment of how the potential flow solver DIFFRACT [17] and the full CFD solver in OpenFOAM [14] perform when applied to non-linear wave interactions with offshore structures for ranges of wave conditions. A single truncated circular column in regular waves with different periods and wave steepnesses has been investigated in the present study as part of the joint international studies organised by the ITTC committee. The sizes of computational domains, complexities of mesh generation, computational time and accuracies of predictions have been taken into account in the comparisons and information is provided in the paper.

A series of model tests for a single truncated circular column in regular waves were performed at MARINTEK, the results of which have been used in an ISSC benchmark study [18, 19]. Numerical results of surface elevations have been compared with the ISSC data set previously [20]. Unfortunately, the experiments at MARINTEK did not include force measurements, so additional experiments have been performed at MOERI as described in [21] using the same truncated circular column. Time histories of surface elevations and wave forces were recorded. Both the potential flow solver DIFFRACT and a full CFD solver in OpenFOAM have been used in the present numerical analyses. A brief introduction to these two numerical packages will be given in section 2. In section 3, the experimental set-up at MOERI [21] and selected waves conditions will be described. In section 4, meshes and details of the numerical wave tank (NWT) used in the present analysis will be introduced. Numerical results have been compared with experimental data from MOERI in section 5. In section 6, some conclusions have been drawn based on the present analysis.

2. Description of numerical models

2.1 Potential flow solver DIFFRACT

Within a potential flow framework, the water is assumed to be an incompressible inviscid fluid with irrotational motion and a scalar velocity potential Φ can be defined in the fluid domain that satisfies the Laplace equation, i.e.

$$\nabla^2 \Phi = 0 \tag{1}$$

Eq. (1) with suitable boundary conditions can be solved by using a boundary element method [22]. In the traditional implementation of the boundary element method for wave diffraction/radiation problems, irregular frequencies will introduce sharp "jumps" in numerical results which have no physical basis. For problems with a single body, it may be easy to identify the irregular frequencies because the results are usually expected to be smooth lines. In the interactions between waves and multiple bodies, it can be very difficult to distinguish the physical interactions and unphysical "jumps" at the irregular frequencies.

In the present paper, the frequency domain potential flow solver DIFFRACT is used, which can eliminate the irregular frequencies by introducing the additional equations and partial discontinuous elements (the approach is described in Sun et al [17]). An interface between the potential flow solver DIFFRACT and the free pre-processor in SALOME [23] has been created to carry out hydrodynamic analysis for any complex fixed or floating structures. The body surface, internal water plane and outer free surface are discretized into quadratic elements. DIFFRACT is able to solve the three-dimensional wave diffraction

and radiation problems up to second order, for which both uni-directional and multi-directional waves can be considered [24, 25]. Of particular relevance to this paper is the study by Zang et al. [24], examining wave scattering from a stationary idealised ship-shaped body, where excellent agreement was obtained between physical experiments at Imperial College and the first-/second-order predictions from DIFFRACT.

2.2 Full CFD solver in OpenFOAM

The OpenFOAM® toolbox can be used to solve both compressible and incompressible versions of the Navier-Stokes equations on finite volume meshes. For an incompressible fluid, the Navier-Stokes equations representing conservation of both mass and momentum [16], can be written as

$$\nabla \cdot \vec{U} = 0 \tag{2}$$

$$\frac{\partial \rho \vec{U}}{\partial t} + \nabla \cdot \left(\rho \vec{U} \vec{U}\right) - \nabla \cdot \left(\mu \nabla \vec{U}\right) - \rho \vec{g} = -\nabla p - \overrightarrow{f_\sigma} \tag{3}$$

Here, ρ is the fluid density, p is the fluid pressure and μ is the dynamic viscosity. $\vec{U}$ is the fluid velocity and $\overrightarrow{f_\sigma}$ is the surface tension. It can be seen that the unknowns p and $\vec{U}$ are coupled in Eq. (2) and (3). Several algorithms are available in OpenFOAM to solve the pressure-velocity coupling [26], such as PISO (Pressure Implicit Splitting Operators), SIMPLE (Semi-Implicit Method for Pressure-Linked Equations) and PIMPLE (merged PISO-SIMPLE). A detailed description of the PISO algorithm can be found in the book of Ferziger and Peric [27]. We use PISO algorithm in our numerical simulations.

In the present study, waves2Foam, a free toolbox is used to generate and absorb free surface water waves [14]. At the inlet boundary (wave making boundary), free surfaces, velocities of water particles and pressure gradient are calculated based on the potential flow solution from user-specified wave theories. Several wave theories are available in this toolbox [28] and Stokes first-order wave theory is used to generate incoming waves in the present analysis. To remove the reflected waves from the outlet boundary and waves reflected from the structures, relaxation zones (active sponge layers) have been incorporated downstream of the wave making boundary and in front of the outlet boundary. An explicit relaxation technique is adopted [14]. The main solver in toolbox waves2Foam is waveFoam which is based on the original implementation of interFoam in OpenFOAM and modifications have been made to allow it to be compatible with the libraries for wave generation and absorption [14]. InterFoam is a full CFD solver within OpenFOAM for two incompressible, isothermal immiscible fluids and uses a VOF (volume of fluid) phase-fraction based on the interface capturing approach [26]. There are also several models

provided in OpenFOAM to simulate turbulence and boundary layer effects, such as Reynolds-Averaged Navier-Stokes (RANS), Large Eddy Simulation, Detached Eddy Simulation (DES) and Direct Numerical Simulation (DNS). In the present work, we use a simple laminar flow model for all simulations.

3. Experimental setup and selected wave conditions

The data used in the present study is taken from the model tests [21] on a truncated surface piercing column performed at MOERI. All information is presented as at full scale after applying Froude scaling to the laboratory data. Thus the radius of the column is taken as r=8.0m (diameter D=2r=16.0m) and the draft is 24.0m. A brief review of the experimental setup will be given here. A top view of selected wave probe locations is shown in Fig. 1. Wave probes were installed in a radial pattern around the column, with a distance from the column wall of 0.2063m (inner circle) and 8m (outer circle). The 10 wave probes were divided into pairs, which were at 0, 45, 90, 135 and 180 degrees to the wave direction. The coordinates of the wave probes are given in Table 1.

Using the potential flow solver DIFFRACT, waves in the range k_0r=0.1~0.7 have been considered in the following analysis (where k_0=2π/L and L is wave length). For simulations using the full CFD solver in OpenFOAM, physical scales are used: incoming waves at period T=7s, 9s and 15s. Corresponding wave numbers in deep water k_0 from the linear dispersion relation are 0.0822 m^{-1}, 0.0497 m^{-1} and 0.0179 m^{-1} (k_0r = 0.657, 0.398 and 0.143). At each wave period, waves with 3 steepnesses (H/L=1/30, 1/16 and 1/10) were chosen. Details of the incident waves can be found in Table 2, where H is wave height and A=H/2. For the wave conditions considered here, and the column with diameter D=16.0m, the Keulegan-Carpenter numbers at the mean water level (KC=2$\pi A/D$) are listed in Table 3, all are sufficiently small that we would expect small contributions from drag to the total measured forces.

4. Meshes for potential flow solver and setup of numerical wave tank

4.1 Meshes for potential flow solver DIFFRACT

As noted in section 2.1, the potential flow solver DIFFRACT is based on the boundary element method. Traditionally, only meshes on the body surface would be needed as shown in Fig.2 (a). Two-plane symmetry has been implemented in the numerical model DIFFRACT to improve computational efficiency while maintaining a high degree of accuracy. To avoid the difficulty of calculating coefficients associated with the exterior solid angle [22], meshes are also generated on the artificial inner free surface inside the body perimeter (e.g. Fig. 2 (b)). For second-order calculations, integrals on the outer free surface are needed. Corresponding meshes can be found in Fig. 2 (c). Generally, converged results are

easy to obtain at first order [29]. Second-order results are very sensitive to the mesh patterns and sizes [17]. The first- and second-order results based on the meshes in Fig.2 have been compared with those from WAMIT for the ISSC benchmark study [18]. Satisfactory agreement is achieved (as shown in Fig. 6.5.2 in the ITTC report [21]). So the meshes shown in Fig.2 were chosen for the following analysis. In total, there are 192 elements on the body surface (in Fig.2 (a)), 64 elements on the inner free surface (in Fig.2 (b)) and 258 elements on the outer free surface (in Fig.2 (c)). Generally, it took ~ 12 minutes to obtain the RAO (Response Amplitude Operator) and QTF (Quadratic Transfer Function) at each regular wave frequency, running DIFFRACT on a single core of a PC.

4.2 Setup for numerical wave tanks (NWT) based on OpenFOAM

To simulate wave-structure interactions using the OpenFOAM toolbox waves2Foam [14], the geometry of the NWT and corresponding meshes have been created by using the free pre-processor in SALOME [23]. The mesh information has been exported from SALOME into an I-deas Universal (UNV) file, which is converted for OpenFOAM by using "ideasUnvToFoam" utility [26]. The lengths of the numerical wave tanks are set as $6L$ (for T=9s and T=15s) *or* $35D$ (for T=7s). At the left end (behind inlet boundary) and right end (in front of outlet boundary) of the NWT, damping zones of $1.5L$ are used to avoid unwanted wave reflection as mentioned in section 2.2. The truncated circular column is placed at the centre of the NWT ($3L$ or $17.5D$ from the inlet boundary). In the selections of the height of the NWT, both wave lengths and wave heights have to be considered. Because the column was tested in deep water [21], water depths in the NWT have been set as $1.0L$ (for T=9s and T=15s) *or* $8D$ (for T=7s). To allow simulation of the interactions between wave and column, sufficient height is required above the mean water level and this is set to $1.25H$ here. The total height of the NWT used in our study is $1.0L$+$1.25H$ (for T=9s and T=15s) or $8D$+$1.25H$ (for T=7s). At the bottom and side walls of the NWT, slip boundary conditions are applied. On the surface of the column, a no-slip boundary is adopted. A combined boundary condition "pressureInletOutletVelocity" [26] is used for the velocity at the upper boundary of the NWT and its pressure is specified as "totalPressure". The pressure conditions for the other boundaries of the NWT are set as "zeroGradient".

Hexahedral cells have been generated at the left and right ends of the NWT. Based on the previous analysis [16], the horizontal sizes of elements are set to about $L/70$. In the vertical direction, at least 8 cells are generated in one wave height H. Prism cells have been used in the central square region around the column and average mesh densities can be determined by the number of cells on the waterline of the column. The widths of the NWT are set as 128m initially and three meshes in the central area are used. Meshes on the surface of the column and around the column with different densities (1:2:3) are shown in

Fig. 3. The corresponding numerical results for surface elevations at "WPB1" (as shown in Table 1, this is just ahead of the front stagnation point of the column) and the total horizontal force on the column can be found in Fig.4 for a wave with T=9s and H/L=1/16. Very small differences are found in the results based on three meshes. Consequently meshes with low density ("Mesh 1" in Fig.3 (a)) are used in the remaining simulations presented in this paper.

To analyse the effects from two side walls of the NWT, another NWT with width of 256m was also created for a wave with T=9s and H/L=1/16. Numerical results of surface elevations at the front stagnation point "WPB1" and horizontal forces on the column in the NWTs with different widths are shown in Fig.5. The differences between the two sets of numerical results in Fig.5 are believed due to the side-wall effects. To ensure the accuracy of the numerical predictions, the wider NWT with width of 256m has been used in the present studies. Of course, more computational time is needed for a wider NWT. For the wave at T=9s with steepness of H/L=1/16, there are 8,293,806 cells in the NWT. For this mesh, usable results for 10 wave periods required about 62 hours running OpenFOAM with 32 cores on the HPC at the University of Bath.

5. Results and discussions

5.1 RAOs and QTFS of surface elevations and wave forces

The RAOs and QTFs of free surface elevations and wave forces for frequency domain analysis are obtained directly using the potential flow solver DIFFRACT. For the time histories of surface elevations and wave forces obtained from experiments and time domain CFD analysis, the contributions of each harmonic component are obtained using Fourier analyses. The RAOs and QTFs of the free surface elevations and wave forces obtained from both the potential flow solver DIFFRACT and the CFD tool OpenFOAM are compared with experimental data from MOERI [21] as shown in Figs. 6-10 and Tables 4-8 for the first- and second-order harmonics. In Table 4-8, the percentage difference between numerical results and experimental measurements is given in the columns next to the numerical results. Obviously, as seen in the tables, the RAOs and QTFs obtained by the frequency domain potential flow solver DIFFRACT do not vary with wave heights.

The comparisons of the RAOs of surface elevations near the column are shown in Figs. 6 and Table 4. Generally, the RAOs from the potential flow solver DIFFRACT agree well with those from experiments for waves with steepness H/L=1/30 except the surface elevations at the downstream quarter point "WPB4" which is believed due to the very strong nonlinear interactions as shown in Fig. 11(c) and

Fig.13. As one might expect, larger discrepancies between numerical results from DIFFRACT and experiments have been found for steeper waves (H/L=1/16 and 1/10). The largest difference is up to 51.0% at "WPB4" for wave at T=9s and H/L=1/10. These discrepancies possibly come from the limitations of linear theory which can only consider the contribution of the first-order term. However, third-order terms may also produce contributions to the first harmonic frequency in experiments for steep waves via nonlinear combinations of components, with possible limitations on this process from local wave breaking for the steepest waves. In most of cases shown in Fig. 6 and Table 4, the full CFD solver in OpenFOAM gives more accurate estimations for steeper waves and the largest difference (-15.9%) is also found at "WPB4" for wave at T=15s and H/L=1/10. Further investigations for more wave cases would be desirable. In the model tests, it is possible that some waves with large steepness have broken when they impact on the column. Turbulence models may be required within the CFD computations to simulate the violent wave-structure interactions in these cases.

The comparisons of the RAOs of surface elevations at the outer circle of wave probes (8.0m to the surface of the column) are shown in Fig. 7 and Table 5. Generally, the accuracy of numerical results is better than those near the column (as listed in Table 4). The largest discrepancy (21.1%) between numerical results of DIFFRACT is found downstream of the column at "WPO4" for waves with T=9s and H/L=1/10. The corresponding largest discrepancy for OpenFOAM is -13.1% at "WPO5" for waves at T=15s and H/L=1/10, which implying that the CFD solver in OpenFOAM has underestimated the RAO of surface elevation at this location.

From the results in Figs. 6 and 7, it is interesting to note that wave interaction with the truncated circular cylinder may result in higher wave run-up near the upstream stagnation point with up to 2× the incoming wave amplitude for short waves. Between the shoulder and rear part of the cylinder (e.g. the downstream quarter point "WPB4"), the wave may only reach 60% of the incoming wave amplitude. This variation is reduced for those points on the outer circle of the wave gauges about one radius away from the cylinder.

In Figs. 8, 9, Tables 6 and 7, the QTFs of surface elevations are presented, which are defined as $\eta^{(2)}r/A^2$. Here $\eta^{(2)}$ is the amplitude of the double frequency second harmonic component (second-order) and r is the radius of the column. The differences of QTFs between numerical results and experimental data are generally larger compared with those of RAOs in Tables 4 and 5. The differences of QTFs are at the range of -73% ~ 128% for surface elevations at the inner circle in Table 6 and -73% ~ 168% for those at the outer circle in Table 7. Relatively smaller discrepancies between numerical results of DIFFRACT and experiments are found for waves with small steepness (H/L=1/30) at the upstream weather side ("WPB1", "WPB2", "WPO1" and "WPO2") in Figs. 8 and 9. Larger difference arises for steeper waves, especially

for the results of surface elevations at the shoulder and leeward side. As shown in the following Figs. 11 and 12, stronger nonlinear interactions are found at the shoulder and leeward side of the column which are beyond the capability of DIFFRACT which can calculate only the first- and second-order components.

In Fig. 10 and Table 8, the first and second harmonics of wave forces are non-dimensionalised using $\rho g A r^2$ and $\rho g A^2 r$ respectively. Similar to the comparisons of surface elevations, better agreement between the numerical results and measurements is found in the RAOs than in the QTFs. It seems that both DIFFRACT and the CFD solver in OpenFOAM can provide relatively more accurate predictions for RAOs and QTFs for horizontal forces than for vertical forces. The largest discrepancies are found in QTFs of vertical forces in Fig. 10 (d). In Fig.10 (a), (c) and Table 8, it can be found that better estimations are provided by DIFFRACT for RAOs and QTFs of the horizontal forces in most of the comparisons although the changes with wave height cannot be considered in DIFFRACT. For RAOs and QTFs of the vertical forces, the accuracy of numerical results from DIFFRACT and the CFD solver in OpenFOAM are comparable. For the potential flow solver DIFFRACT, the discrepancies may be due to the higher-order contributions beyond second order and the limitations of the inviscid assumption. For the CFD solver in OpenFOAM, more investigations are needed to check the consequences of including turbulence models. There are also some concerns from the analyses of experimental data for wave forces. As shown in Fig. 14(b) (discussed further below), obvious high frequency oscillations are found in the measurements of vertical forces. In the numerical models, the truncated circular column can be fixed rigidly. However, the column was connected to a carriage in the experiments (as shown in Fig. 6.2.1.2 in the ITTC report [21]), which may suggest that it was not constrained ideally. High frequency components due to the structural dynamic responses of the column may have polluted the measurements of the hydrodynamic forces [30], which may have affected estimates of the QTFs (especially for waves with T=7s).

5.2 Surface elevations at wave probes and scattered wave fields around column (T=9s, H/L=1/16)

As mentioned in the previous section, contributions above the second order have to be considered if more accurate predictions for steep wave impact are needed. A wave at T=9s with steepness of H/L=1/16 has been chosen for further analysis here. In Fig. 11, the time histories of numerical results for free surface elevations at 3 locations (“WPB2”, “WPB3” and “WPB4”) near the shoulder of the column have been plotted together with experimental data from MOERI [21]. In Fig. 11(a), the results obtained from the potential flow solver are comparable to those from the CFD solver in OpenFOAM. Strong nonlinear behaviour is found in the measurements at “WPB3” and “WPB4”. Clearly, numerical results based on the full CFD solver in OpenFOAM can give better agreement with experiment than the potential flow model in Figs.11 (b) and (c). Another way of presenting the comparisons is through the corresponding results

from the Fourier analysis shown in Figs. 11(d), (e) and (f). Of course, the potential flow solver DIFFRACT can only be used to predict contributions up to second order - those at the difference frequency of zero, the linear and double frequency. However, OpenFOAM is able to predict the contributions beyond the second order which may have significant effects on the accuracy of the numerical simulations, especially at the column shoulder (point "WPB3") and lee side (point "WPB4"), where the third and fourth harmonic components can be clearly seen in the spectra.

The time histories of the surface elevations at the points "WPO2", "WPO3" and "WPO4", one radius (8.0m) away from the body surface, and the corresponding spectra are shown in Fig. 12. It can be seen that both the potential flow solver and the full CFD solver in OpenFOAM can give accurate predictions at point "WPO2". For point "WPO3", the full CFD solver can provide better agreement with experiment at the crests, but less accurate estimations of the troughs than those obtained from the potential flow solver. For point "WPO4", the full CFD solver has provided better predictions for both crests and troughs.

From the amplitude spectra in Figs. 11 and 12, it can be seen that nonlinear effects become stronger going from weather side ("WPB2" and "WPO2") to lee side ("WPB4" and "WPO4") of the column, higher order harmonics providing greater contributions. The full CFD solver has provided reasonable estimates of the experimentally measured behaviour up to the fourth harmonic.

Traditionally, interactions between waves and a column are assumed to depend on D/L (here D is the diameter of the column and L is wave length). If the body is small, $D/L<0.2$, the flow lies within the drag-inertia regime and the body is assumed to cause little or no disturbance to the incident wave field (except for the local phenomena of flow separation and wake formation behind the column). For the present case with $D/L=0.13$ (as shown in Table 2), however, significant higher-order contributions to surface elevations have been found at the shoulder and down-wave side of the column (as shown in Figs. 11 and 12). Possible explanations can be found in the physical experiments reported by Swan and Sheikh [31], in which the origins of high-frequency wave scattering were linked to the circulation of fluid around the column. Also relevant is the four-phase contribution analysis reported by Fitzgerald et al. [32], their analysis showing the scattered wave components at each harmonic up to the fourth. Relevant to the structure of the local scattered field are the observations of a secondary load cycle for large waves passing a cylinder made by Grue and Huseby [33], with locally very steep short wave components being observed. These will not be accurately captured by the second-order calculations of DIFFRACT but should be in the fully nonlinear CFD results.

To give better understanding of the current case, the scattered wave fields (which is in an area of 200m=12.5D by 256m=16D) obtained by the full CFD solver in OpenFOAM have been plotted in Fig. 13 at intervals of $\Delta t \approx T/4$. When the wave crest approaches the column at t=69.05s in Fig. 13, Type-1 scattered wave fields specified by Swan and Sheikh [31] have been observed in front of the column, which correspond to concentric wave fields. Then the surface elevation at the front stagnation point "WPB1" reaches its maximum value when the wave crest impacts the column at t=71.35s. Type-2 scattered wave fields [31] have developed at the shoulders of the column, which are non-concentric wave fields. In the far field in front of the column, concentric patterns still exist. At t=73.55s, the wave crest has passed the column, and non-concentric (Type-2) wave fields have moved downstream of the column. When the wave trough approaches the column at t=75.85s, Type-1 scattered wave fields have been observed again. From the whole process, it can be seen that the Type-2 modes occur around the shoulders of the column and the down-wave side, which may induce higher-order contribution to the elevations in these area as suggested previously. In Fig. 13, transverse waves may also be noted (though we have confirmed that the numerical wave tank is sufficiently wide that reflections from the side walls do not significantly influence the wave field at the locations where these components are seen).

5.3 Time histories and amplitude spectra of forces for a wave at T=9s with steepness of H/L=1/16

For the same case of a wave at T=9s with a steepness of H/L=1/16, the time histories of horizontal and vertical wave forces on the column and the corresponding amplitude spectra are compared in Fig.14. It is clear that nonlinearity in the wave force is not as strong as in the results of surface elevations (as shown in Figs. 11 and 12), this being especially noticeable for horizontal forces. The surface elevations at different locations show the local behaviour during the wave-structure interactions. However, these local effects are mostly integrated out in the measurements and calculations of the wave forces on the column. Both DIFFRACT and OpenFOAM gave reasonable predictions as seen in the horizontal forces in Fig.14. Obvious noise can be observed in the experimental measurement of the vertical force (but the reduced magnitude of the predicted vertical forces should be noted). This noise may be related to the details of the experimental set-up, as discussed at the end of section 5.1.

Apart from the contributions from higher-order harmonics discussed in the present paper, for which an irrotational flow model appears to be appropriate, possible viscous contributions to the flow field (drag and flow separation) [34] clearly require comment. For the current cases in deep water, the Keulegan-Carpenter numbers at the mean water level are relatively small (as shown in Table 3). Flow separation is usually assumed to be important for prediction of forces when KC numbers are higher than 6. However, it has also been argued that flow separation may occur at lower KC numbers [35]. Further investigation of

simulations of the full Navier-Stokes equations are warranted, though the importance of viscous effects on the free surface elevations remains unclear.

6. Conclusions

Free surface elevations around a fixed truncated column and horizontal/vertical forces on the column have been investigated in the present paper. Both the potential flow solver DIFFRACT and the full CFD solver in OpenFOAM have been used in the numerical simulations to assess their capabilities. In the case of the potential flow solver DIFFRACT, only relatively coarse meshes are needed to provide converged results. But much more user and computational effort is required for simulations using the full CFD solver to achieve converged and accurate results, with very fine meshes for both horizontal and vertical directions. To compare the accuracy of each numerical solver, the results have been compared with data from experiments [21] for waves of different wave periods and steepnesses. This analysis includes a detailed examination of the surface elevation structure for a regular wave at period T=9s with steepness of H/L=1/16, including harmonic analysis of the experimental and full CFD data up to the fourth harmonic.

In most of the cases, reasonable agreement has been obtained between the results from the efficient second-order frequency domain potential flow solver DIFFRACT and the experimental data, especially (as expected) for waves with small steepness. However, it seems that DIFFRACT is unable to provide accurate predictions for cases of elevation with steep incident waves, even for the results at the first harmonic. This may imply that for steep waves linear potential flow theory may significantly underestimate first harmonic free surface elevations near the front stagnation points, locations "WPB1" and "WPB2", while overestimating these elevations near points between the shoulders and the rear stagnation point, location "WPB4". The discrepancies appear to arise because of the limitation of the small amplitude assumption and the absence of higher-harmonic contributions beyond second order.

Compared with the second-order potential theory applied in the frequency domain, the full CFD solver in OpenFOAM required several orders of magnitude more computational time and a large number of cells in the numerical domain. However, significantly more accurate predictions can be obtained for situations with large incoming waves, with the ability to model contributions beyond the second harmonic. From the comparisons with experiments at MOERI, reasonable agreement has been achieved up to the fourth harmonic. And the predicted spatial structures of the scattered wave fields close to the column, obtained from the full CFD solver, are consistent with the Type-1 and Type-2 patterns observed in physical mode tests by Swan and Sheikh at Imperial College [31].

Acknowledgements

This work was carried out within the research project SMARTY - Supergen Marine Technology Challenge (EP/J010316/1) which has been funded by the UK Engineering and Physical Sciences Research Council (EPSRC). The financial support from the EPSRC is greatly appreciated. The computations were performed on the University of Bath's High Performance Computing Facility. Provision of services by BUCS HPC Support Team is gratefully acknowledged. The authors would also like to thank Prof. Wei Qiu and the Ocean Engineering Committee of the 27th International Towing Tank Conference for providing the experimental data in this work.

References

[1] McCamy R, Fuchs R. Wave forces on piles: a diffraction theory. Tech. Memo No. 69, Beach Erosion Board, U.S. Army Corps of Engineers, Washington D.C., USA, 1954.

[2] Eatock Taylor R, Hung SM. Second order diffraction forces on a vertical cylinder in regular waves. Applied Ocean Research 1987; 9(1): 19-30.

[3] Eatock Taylor R, Chau, FP. Wave diffraction - some developments in linear and non-linear theory. Journal of Offshore Mechanics and Arctic Engineering, 1992; 114, 185–194.

[4] Lee CH, Newman JN. Computation of wave effects using the panel method. Numerical Models in Fluid–Structure Interaction, WIT Press, Southampton, 2005, pp. 211–251.

[5] Teng B, Kato S. Third order wave force on axisymmetric bodies. Ocean Engineering 2002; 29(7): 815-843.

[6] Bai W, Feng X, Eatock Taylor R, Ang KK. Fully nonlinear analysis of near-trapping phenomenon around an array of cylinders. Applied Ocean Research 2014; 44: 71-81.

[7] Yan S, Ma Q, Cheng, X. Numerical investigations on transient behaviours of two 3-D freely floating structures by using a fully nonlinear method. Journal of Marine Science and Applications 2012; 11(1):1-9.

[8] Wang CZ, Wu GX. Interactions between fully nonlinear water waves and cylinder arrays in a wave tank. Ocean Engineering 2010; 37(4):400-417.

[9] Ferrant P. Fully nonlinear interactions of long-crested wave packets with a three dimensional body. In: Proceedings of the 22nd Symposium on Naval Hydrodynamics. 1998. p. 403-415.

[10] Yang C, Ertekin RC, Numerical simulation of nonlinear wave diffraction by a vertical cylinder. Transactions of ASME, Journal of Offshore Mechanics and Arctic Engineering 1992; 114(1):36-44.

[11] Lu L, Chen XB. Dissipation in the gap resonance between two bodies. In: Proceedings of 27th International Workshop on Water Waves and Floating Bodies, Copenhagen, Denmark, 2012. http://www.iwwwfb.org/Abstracts/iwwwfb27/iwwwfb27_28.pdf (accessed 24.11.2015)

[12] Darvishzadeh T, Sari A. CFD Applications in Offshore Engineering. In: Offshore Technology Conference, 04-07 May, Houston, Texas, USA, 2015, OTC-25930-MS.

[13] Morgan G, Zang J, Greaves, DM, Heath, A, Whitlow, C, Young, J. Using the rasInterFoam CFD model for wave transformation and coastal modelling, In: Proceedings of 32nd Conference on Coastal Engineering, Shanghai, China, 2010.

[14] Jacobsen NG, Fuhrman DR, Fredsøe J. A wave generation toolbox for the open-source CFD library: OpenFoam®. International Journal for Numerical Methods in Fluids 2012; 70(9): 1073-1088.

[15] Higuera P, Lara, JL, Losada IJ. Simulating coastal engineering processes with OpenFOAM. Coastal Engineering 2013; 71: 119-134.

[16] Chen LF, Zang J, Hillis A, Morgan G., Plummer AR. Numerical investigation of wave-structure interaction using OpenFOAM. Ocean Engineering 2014; 88: 91-109.

[17] Sun L, Eatock Taylor R, Taylor PH. Wave driven free surface motion in the gap between a tanker and an FLNG barge. Applied Ocean Research, 2015; 51: 331-349.

[18] Kristiansen T, Baarholm R, Stansberg CT. Validation of second-order analysis in predicting diffracted wave elevation around a vertical circular cylinder. In: Proceedings of the 14th International Offshore and Polar Engineering Conference, Toulon, France, 2004, p. 342-349.

[19] Nielsen FG. Comparative study on airgap under floating platforms and run-up along platform columns. Marine Structures 2003; 16(2): 97-134.

[20] Sun L, Chen L, Zang J, Eatock Taylor R, Taylor, PH. Nonlinear interactions of regular wave with truncated circular column. In: Proceedings of ITTC (International Towing Tank Conference) Nantes Workshop on Wave Run-up and Vortex Shedding, Nantes, France, 2013.

[21] Ocean Engineering Committee. Final Report and Recommendations to the 27th ITTC, Copenhagen, Denmark, 2014.

[22] Chau FP. The second order velocity potential for diffraction of waves by fixed offshore structures. Ph.D. thesis, University of London. Department of Mechanical Engineering, University College London, Report OEG/89/1; 1989.

[23] OPEN CASCADE. SALOME – The Open Source Integration Platform for Numerical Simulation. http://www.salome-platform.org (accessed 24.11.2015)

[24] Zang J, Gibson R, Taylor PH, Eatock Taylor R, Swan C. Second order wave diffraction around a fixed ship-shaped body in unidirectional steep waves. Transactions of ASME, Journal of Offshore Mechanics and Arctic Engineering 2006; 128(2): 89-99.

[25] Sun L, Zang J, Eatock Taylor R, Taylor PH. Effects of wave spreading on performance of a wave energy converter. In: Proc of the 29th International Workshop on Water Waves and Floating Bodies, Osaka, Japan, 2014. http://www.iwwwfb.org/Abstracts/iwwwfb29/iwwwfb29_51.pdf (accessed 24.11.2015)

[26] Greenshields CJ. OpenFOAM User Guide (Version 2.4.0). OpenFOAM Foundation Ltd, 2015.

[27] Ferziger JH, Peric, M. Computational Methods for Fluid Dynamics, 3rd Edition. Springer, Berlin, 2002.

[28] Jacobsen NG. OpenFOAMWiki. https://openfoamwiki.net/index.php/Contrib/waves2Foam (accessed 24.11.2015).

[29] Birknes J. A convergence study of second-order wave elevation on four cylinders. In: Proceedings of the 11th International Offshore and Polar Engineering Conference, Stavanger, Norway, 2001, p. 392-399.

[30] Mclaughlan, S. Wave Loading On Offshore Wind Turbine Columns. Report for the Fourth-year Project, Department of Engineering Science, University of Oxford, 2011.

[31] Swan C, Sheikh R. The interaction between steep waves and a surface-piercing column. Phil. Trans. R. Soc. A 2015; 373 (2033), DOI:10.1098/rsta.2014.0114.

[32] Fitzgerald C, Taylor PH, Eatock Taylor R, Grice JR, Zang J. Phase manipulation and the harmonic components of ringing forces on a surface-piercing column. Proc Roy Soc Lond Ser A - Math Phys Eng Sci 2014; 470(2168):20130847

[33] Grue J, Huseby M. Higher-harmonic wave forces and ringing of vertical cylinders. Applied Ocean Research 2002; 24(4): 203-214.

[34] Stansberg CT, Kristiansen T. Non-linear scattering of steep surface waves around vertical columns. Applied Ocean Research 2005; 27(2): 65-80.

[35] Trulsen K, Teigen P. Wave scattering around a vertical cylinder: fully nonlinear potential flow calculations compared with low order perturbation results and experiments. In: Proceedings of the 21st International Conference on Offshore Mechanics and Arctic Engineering (OMAE 2002), Oslo, Norway, 2002.

Lists of figures

List of tables

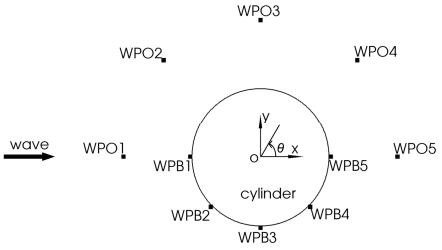

Fig. 1 Layout of wave probes at MOERI

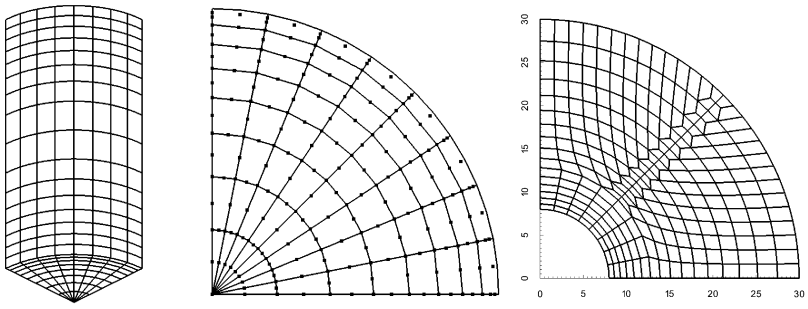

(a) (b) (c)

Fig.2 Meshes for DIFFRACT (a) body surface (b) inner free surface (c) outer free surface

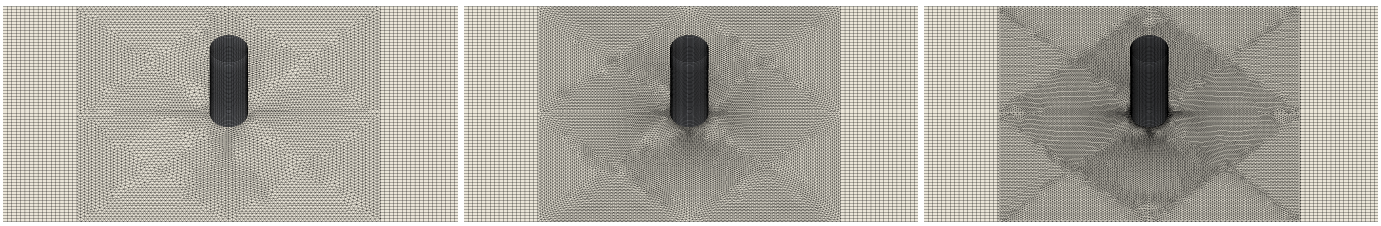

(a) (b) (c)

Fig.3 Local meshes near the column in NWT with width of 128m (a) Mesh 1 (b) Mesh 2 (c) Mesh 3

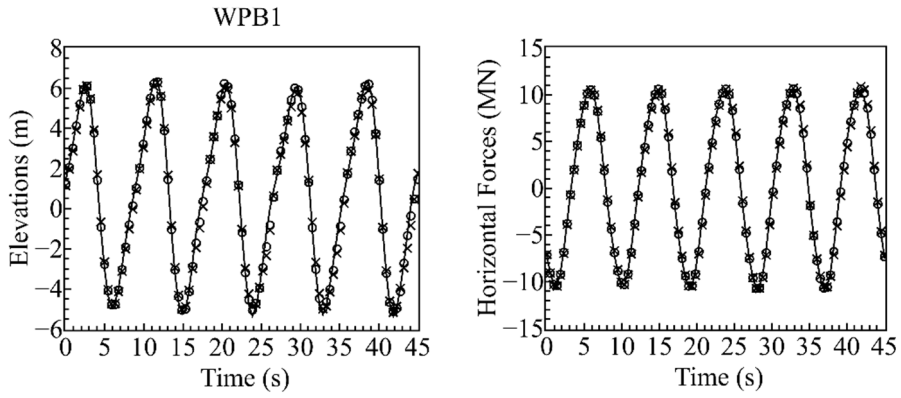

(a) (b)

Fig.4 Numerical results based on different meshes (a) elevation at WPB1 (b) horizontal forces on column

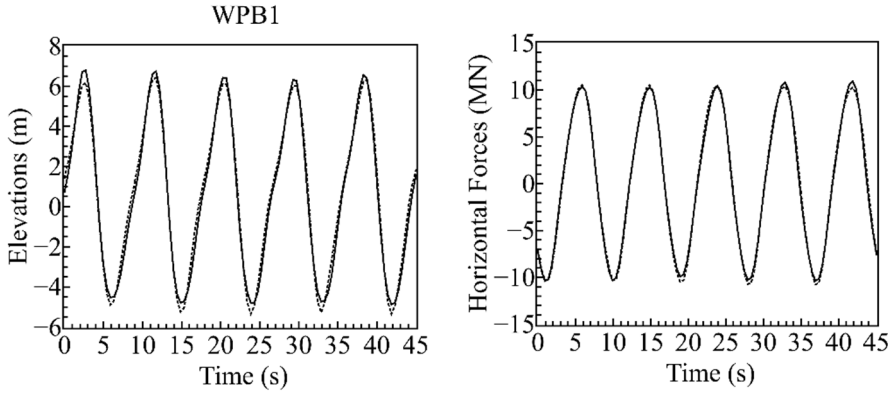

(a) (b)

Fig.5 Numerical results based on different widths of NWT (a) elevation at WPB1 (b) horizontal forces on column

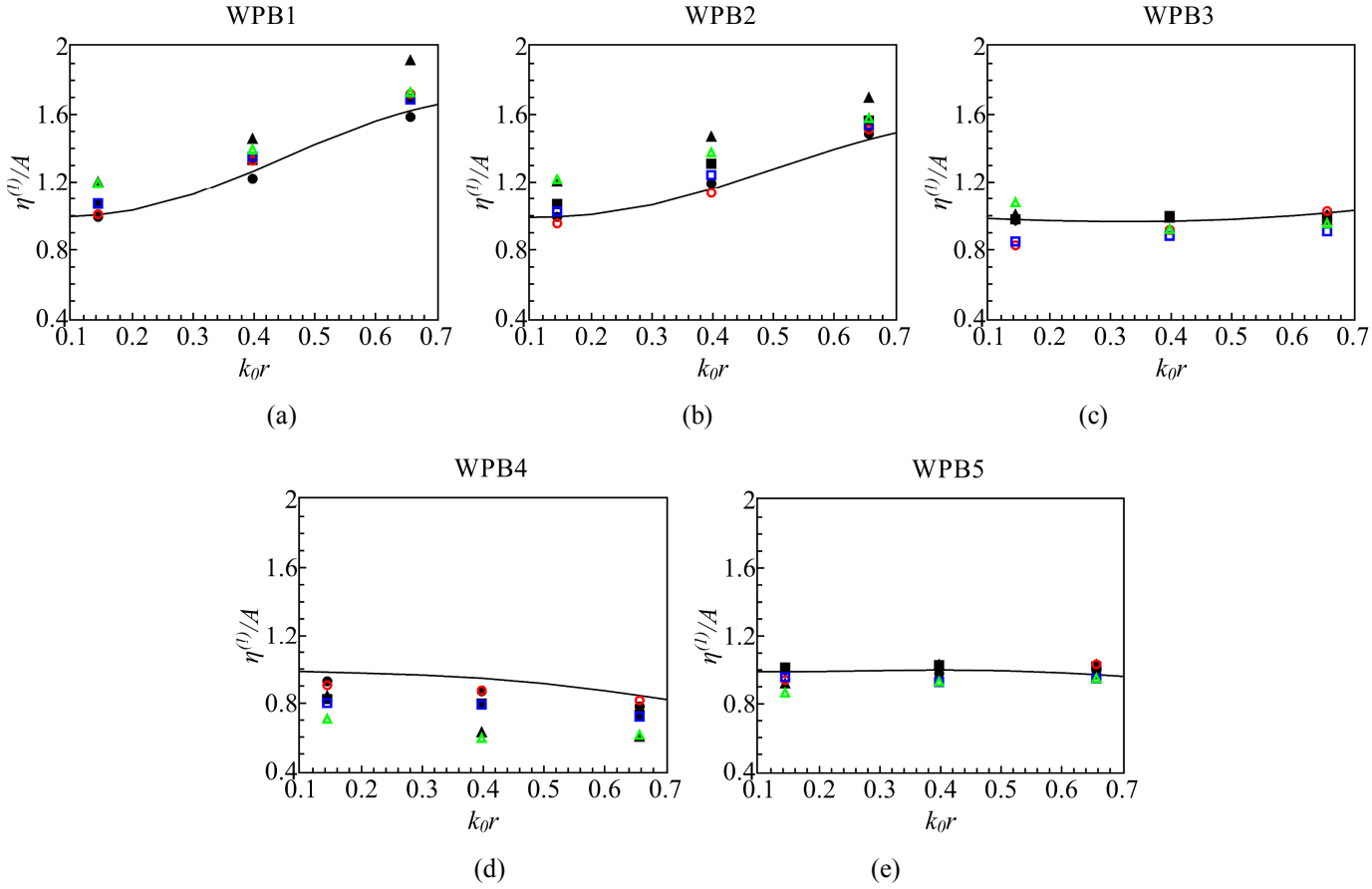

Fig.6 RAOs (1st harmonics) of surface elevations at the inner circle of wave probes (see Table 1)

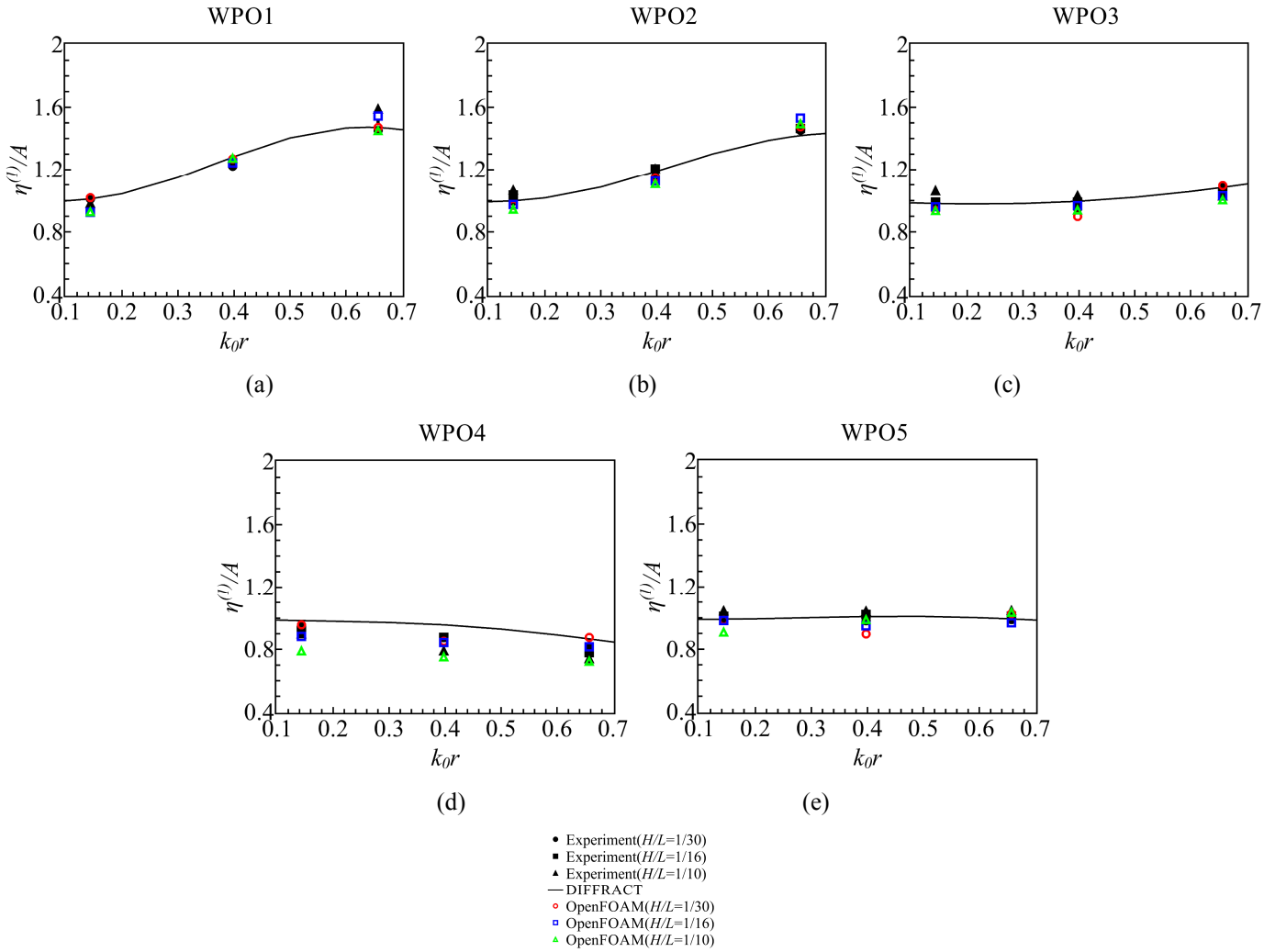

Fig.7 RAOs (1st harmonics) of surface elevations at the outer circle of wave probes (see Table 1)

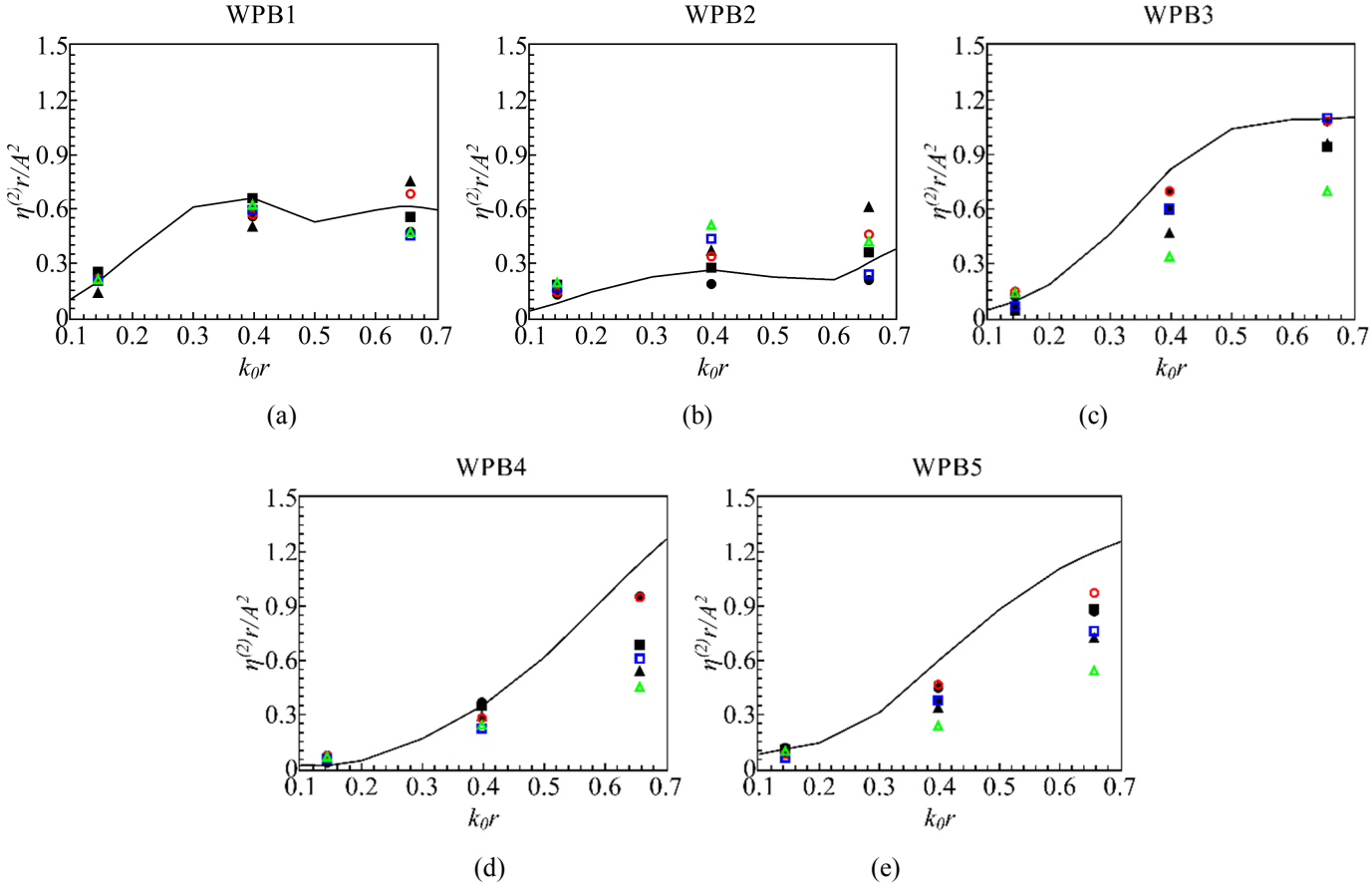

Fig.8 QTFs (2nd harmonics) of surface elevations at the inner circle of wave probes (see Table 1)

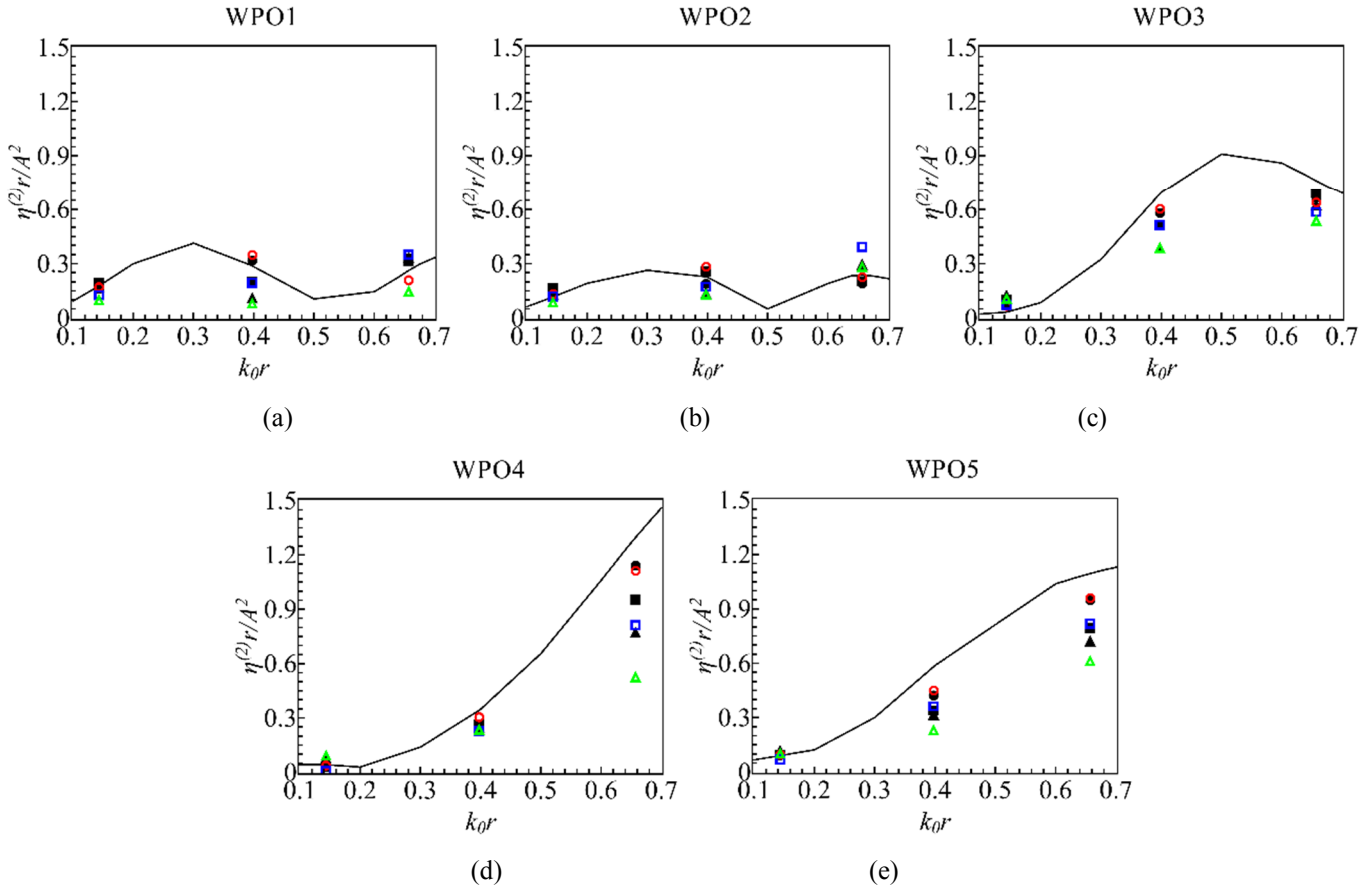

Fig.9 QTFs (2nd harmonics) of surface elevations at the outer circle of wave probes (see Table 1)

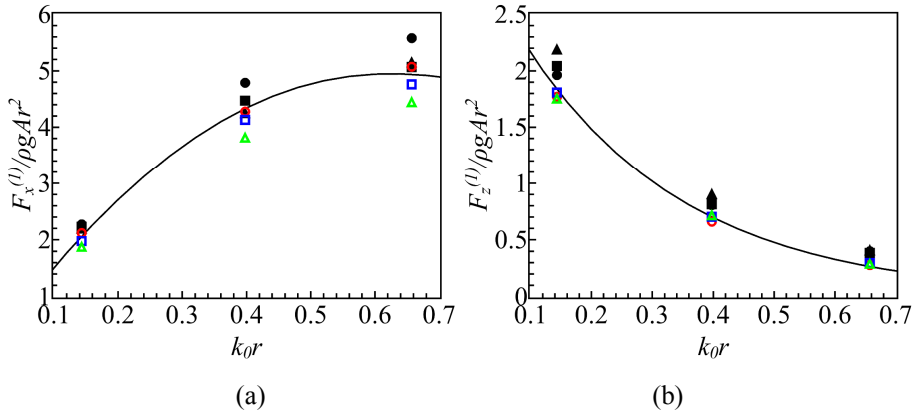

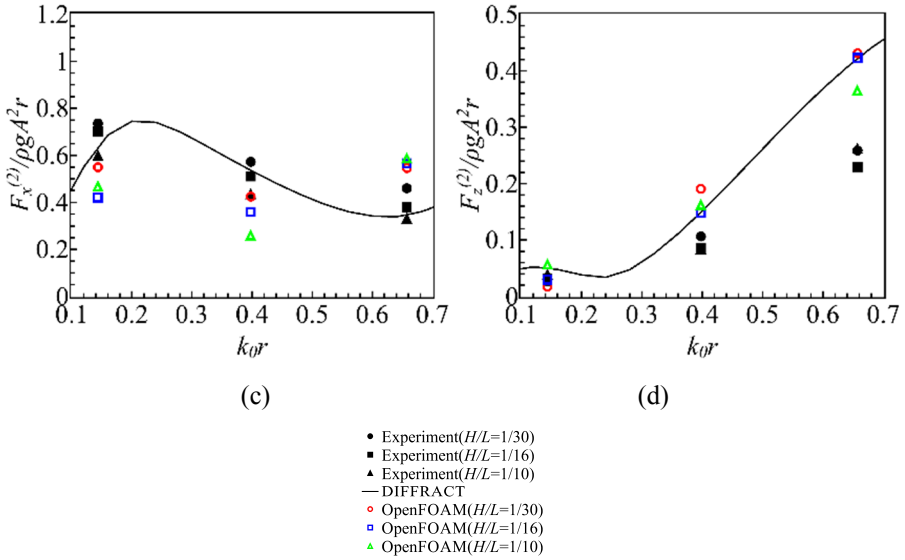

Fig.10 RAOs (1st harmonics) and QTFs (2nd harmonics) of wave forces

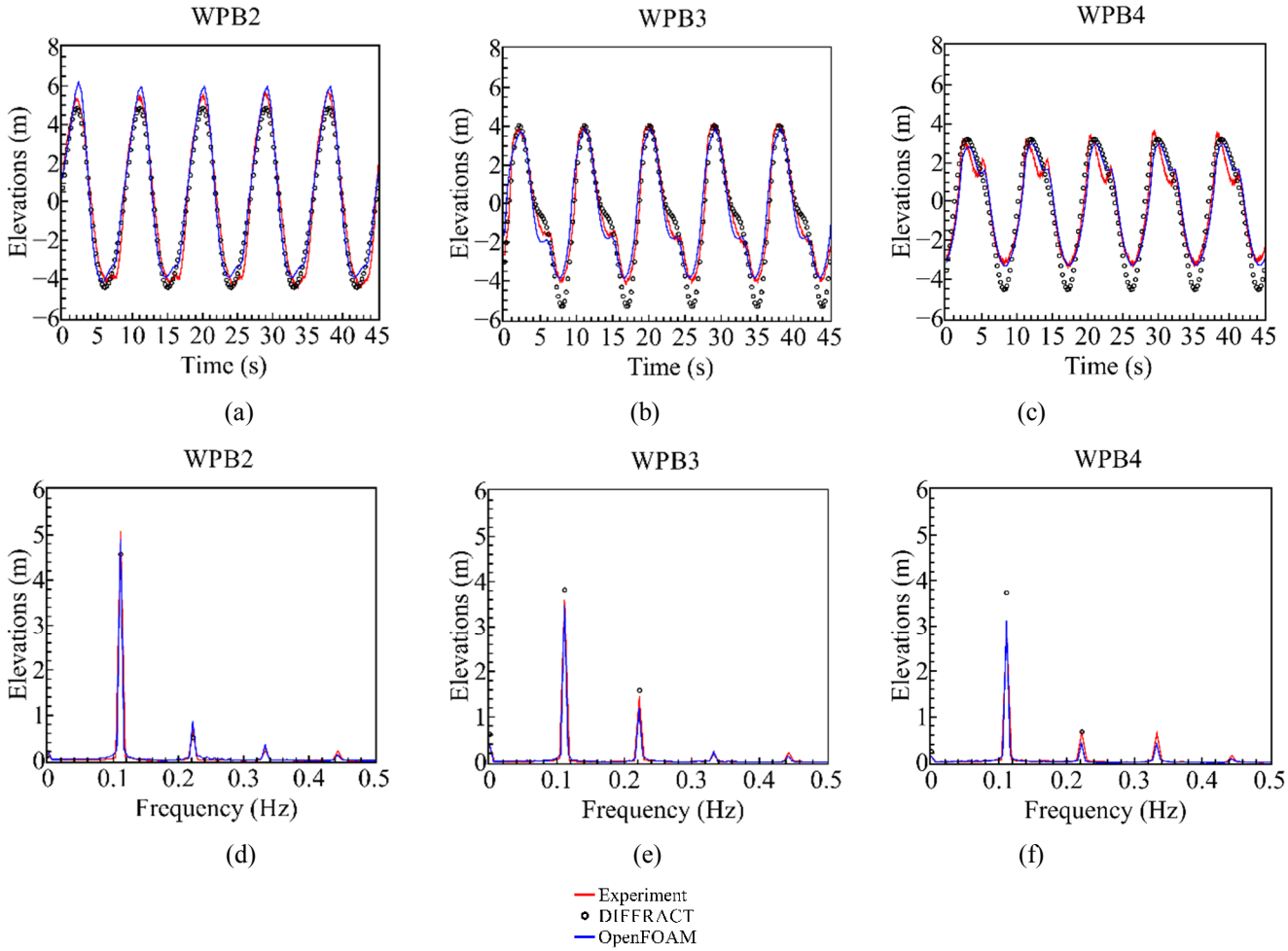

Fig.11 Time histories and amplitude spectra of surface elevations at the inner circle of wave probes (see Table 1)

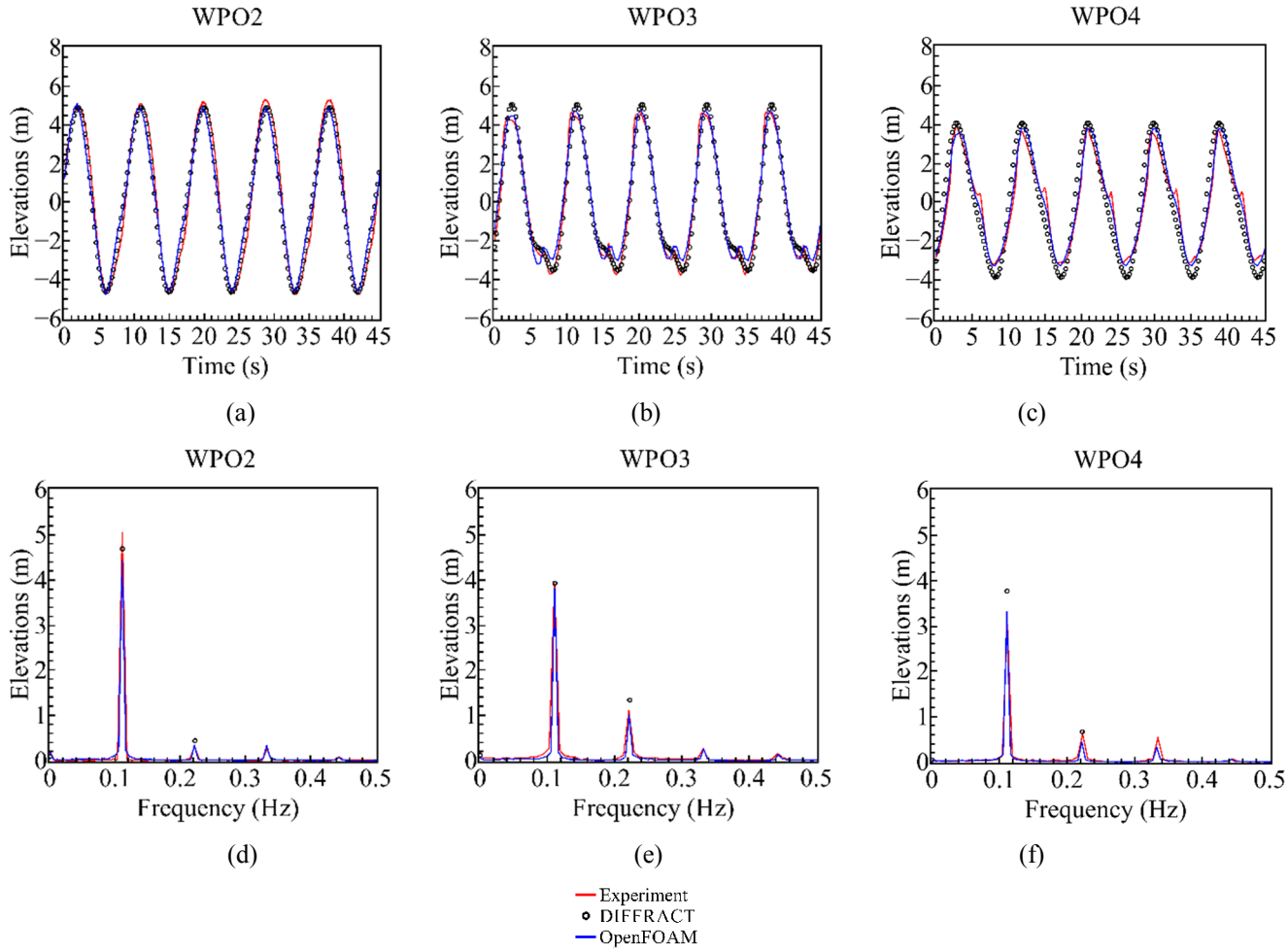

Fig.12 Time histories and amplitude spectra of surface elevations at the outer circle of wave probes (see Table 1)

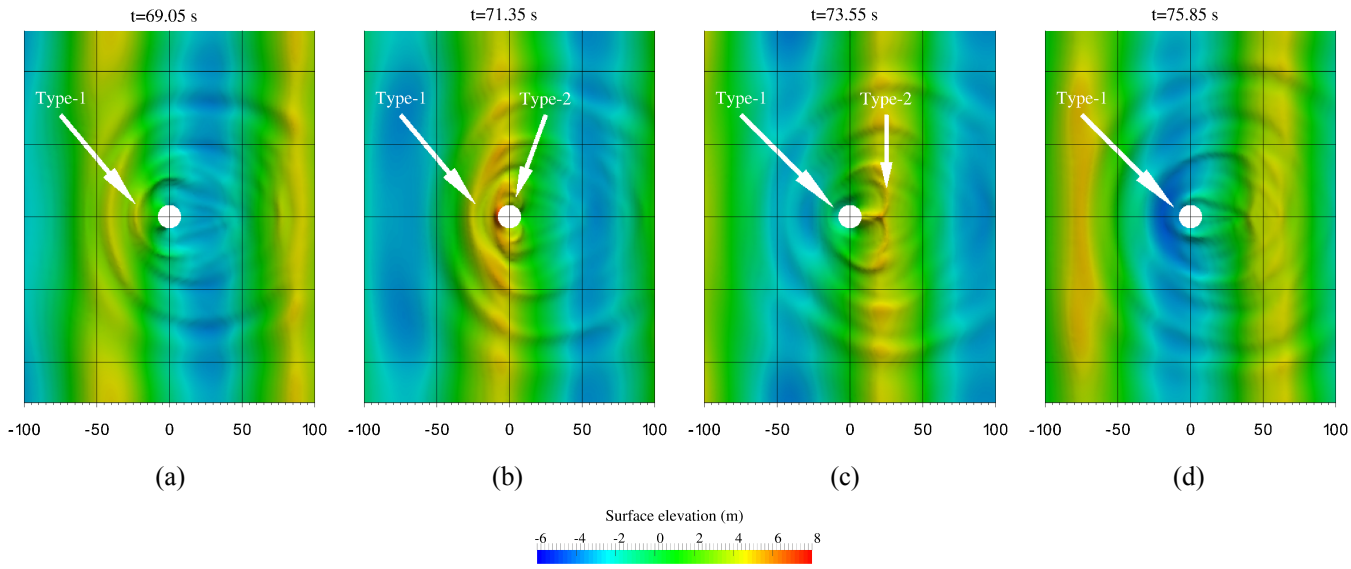

Fig.13 Scattered wave fields around column for wave at T=9s and H/L=1/16

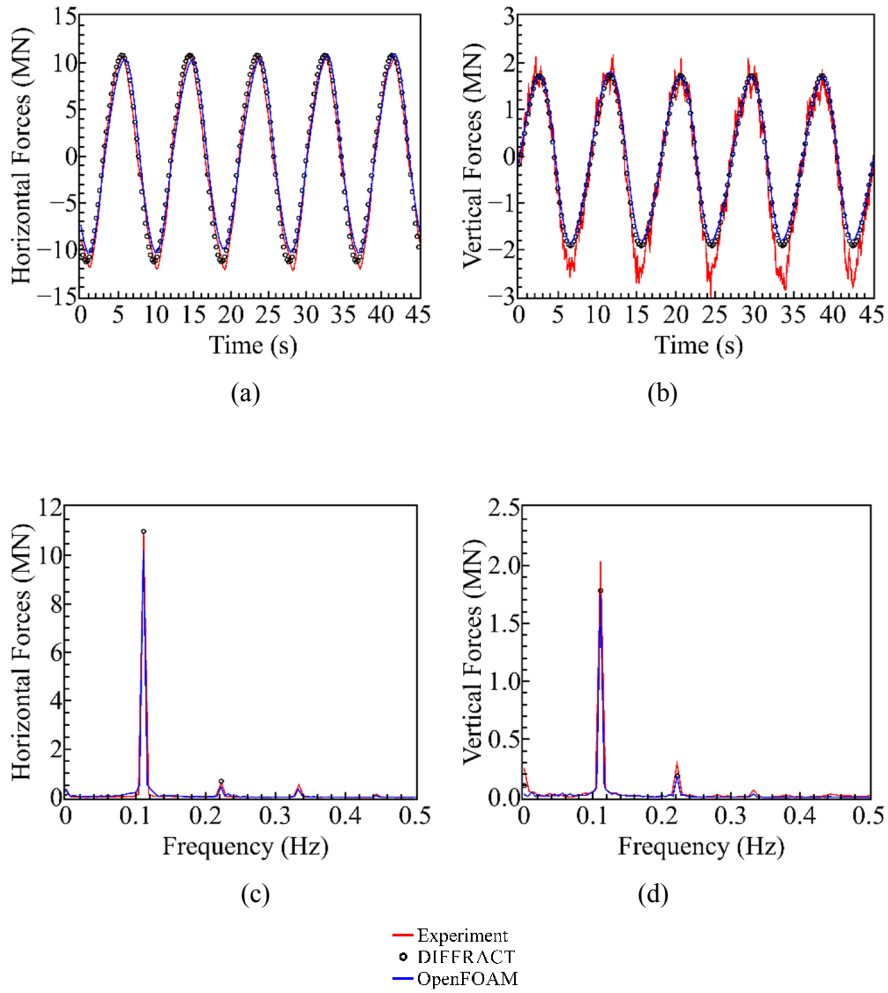

Fig.14 Time histories and amplitude spectra of forces

Table 1 Locations of wave probes (origin is defined at the centreline of the column)

Inner circle	x(m)	y(m)	Outer circle	x(m)	y(m)
WPB1	-8.2063	0.0000	WPO1	-16.0000	0.0000
WPB2	-5.8027	-5.8027	WPO2	-11.3137	11.3137
WPB3	0.0000	-8.2063	WPO3	0.0000	16.0000
WPB4	5.8027	-5.8027	WPO4	11.3137	11.3137
WPB5	8.2063	0.0000	WPO5	16.0000	0.0000

Table 2 Selected wave conditions

		T=7s				*T*=9s				*T*=15s			
H/L	k_0A	*L* (m)	*D/L*	*H* (m)	*A* (m)	*L* (m)	*D/L*	*H* (m)	*A* (m)	*L* (m)	*D/L*	*H* (m)	*A* (m)
1/30	0.1	76.44	0.21	2.548	1.274	126.36	0.13	4.212	2.106	351.00	0.046	11.700	5.850
1/16	0.2			4.777	2.388			7.898	3.949			21.938	10.969
1/10	0.3			7.644	3.822			12.636	6.318			35.100	17.550

Table 3 *KC* numbers for selected wave conditions

	T=7s		*T*=9s		*T*=15s	
	A (m)	*KC*	*A* (m)	*KC*	*A* (m)	*KC*
H/L=1/30	1.274	0.5003	2.106	0.8270	5.850	2.2973
H/L=1/16	2.388	0.9381	3.949	1.5508	10.969	4.3074
H/L=1/10	3.822	1.5009	6.318	2.4811	17.550	6.8919

Table 4 RAOs (1st harmonics) of surface elevations at the inner circle of wave probes (see Table 1)

Wave probes			WPB1	Difference	WPB2	Difference	WPB3	Difference	WPB4	Difference	WPB5	Difference
T=7s	*H/L*=1/30	Experiment	1.586		1.487		1.026		0.782		0.974	
		DIFFRACT	1.622	2.3%	1.453	-2.3%	1.017	-0.9%	0.844	7.9%	0.972	-0.2%
		OpenFOAM	1.722	8.6%	1.513	1.7%	1.028	0.2%	0.816	4.3%	1.034	6.2%
	H/L=1/16	Experiment	1.691		1.566		0.990		0.730		1.022	
		DIFFRACT	1.622	-4.1%	1.453	-7.2%	1.017	2.7%	0.844	15.6%	0.972	-4.9%
		OpenFOAM	1.690	-0.1%	1.540	-1.7%	0.909	-8.2%	0.721	-1.2%	0.951	-6.9%
	H/L=1/10	Experiment	1.918		1.698		0.975		0.601		1.031	
		DIFFRACT	1.622	-15.4%	1.453	-14.4%	1.017	4.3%	0.844	40.4%	0.972	-5.7%
		OpenFOAM	1.731	-9.7%	1.579	-7.0%	0.955	-2.1%	0.613	2.0%	0.951	-7.8%
T=9s	*H/L*=1/30	Experiment	1.223		1.195		0.970		0.871		0.979	
		DIFFRACT	1.264	3.4%	1.158	-3.1%	0.967	-0.3%	0.947	8.7%	1.000	2.1%
		OpenFOAM	1.329	8.7%	1.135	-5.0%	0.918	-5.4%	0.876	0.6%	0.932	-4.8%
	H/L=1/16	Experiment	1.333		1.310		0.999		0.798		1.028	
		DIFFRACT	1.264	-5.2%	1.158	-11.6%	0.967	-3.2%	0.947	18.7%	1.000	-2.7%
		OpenFOAM	1.353	1.5%	1.240	-5.3%	0.880	-11.9%	0.789	-1.1%	0.926	-9.9%
	H/L=1/10	Experiment	1.456		1.468		0.988		0.627		1.031	
		DIFFRACT	1.264	-13.2%	1.158	-21.1%	0.967	-2.1%	0.947	51.0%	1.000	-3.0%
		OpenFOAM	1.395	-4.2%	1.377	-6.2%	0.921	-6.8%	0.595	-5.1%	0.932	-9.6%
T=15s	*H/L*=1/30	Experiment	0.994		0.994		0.952		0.929		1.000	
		DIFFRACT	1.006	1.2%	0.994	0.0%	0.978	2.7%	0.982	5.7%	0.990	-1.0%
		OpenFOAM	1.010	1.6%	0.955	-3.9%	0.828	-13.0%	0.906	-2.5%	0.941	-5.9%
	H/L=1/16	Experiment	1.071		1.069		0.979		0.824		1.015	
		DIFFRACT	1.006	-6.1%	0.994	-7.0%	0.978	-0.1%	0.982	19.2%	0.990	-2.5%
		OpenFOAM	1.074	0.3%	1.026	-4.0%	0.849	-13.3%	0.801	-2.8%	0.959	-5.5%
	H/L=1/10	Experiment	1.203		1.206		1.005		0.841		0.920	
		DIFFRACT	1.006	-16.4%	0.994	-17.6%	0.978	-2.7%	0.982	16.8%	0.990	7.6%
		OpenFOAM	1.197	-0.5%	1.219	1.1%	1.078	7.3%	0.707	-15.9%	0.865	-6.0%

Table 5 RAOs (1st harmonics) of surface elevations at the outer circle of wave probes (see Table 1)

Wave probes			WPO1	Difference	WPO2	Difference	WPO3	Difference	WPO4	Difference	WPO5	Difference
		Experiment	1.453		1.453		1.081		0.813		0.990	
	H/L=1/30	DIFFRACT	1.471	1.2%	1.419	-2.3%	1.084	0.3%	0.867	6.6%	0.993	0.3%
		OpenFOAM	1.472	1.3%	1.476	1.6%	1.097	1.5%	0.877	7.9%	1.027	3.7%
		Experiment	1.511		1.466		1.044		0.780		1.011	
T=7s	*H/L*=1/16	DIFFRACT	1.471	-2.6%	1.419	-3.2%	1.084	3.8%	0.867	11.2%	0.993	-1.8%
		OpenFOAM	1.545	2.3%	1.531	4.4%	1.032	-1.1%	0.817	4.7%	0.968	-4.3%
		Experiment	1.588		1.483		1.030		0.740		1.046	
	H/L=1/10	DIFFRACT	1.471	-7.4%	1.419	-4.3%	1.084	5.2%	0.867	17.2%	0.993	-5.1%
		OpenFOAM	1.450	-8.7%	1.495	0.8%	1.005	-2.4%	0.725	-2.0%	1.034	-1.1%
		Experiment	1.224		1.156		0.950		0.876		0.982	
	H/L=1/30	DIFFRACT	1.281	4.7%	1.188	2.8%	0.995	4.7%	0.957	9.2%	1.008	2.6%
		OpenFOAM	1.270	3.8%	1.150	-0.5%	0.899	-5.4%	0.853	-2.6%	0.898	-8.6%
		Experiment	1.269		1.206		0.991		0.877		1.022	
T=9s	*H/L*=1/16	DIFFRACT	1.281	0.9%	1.188	-1.5%	0.995	0.4%	0.957	9.1%	1.008	-1.4%
		OpenFOAM	1.246	-1.8%	1.124	-6.8%	0.965	-2.6%	0.843	-3.9%	0.944	-7.6%
		Experiment	1.273		1.204		1.030		0.790		1.042	
	H/L=1/10	DIFFRACT	1.281	0.6%	1.188	-1.3%	0.995	-3.4%	0.957	21.1%	1.008	-3.3%
		OpenFOAM	1.274	0.1%	1.109	-7.9%	0.940	-8.7%	0.753	-4.7%	0.988	-5.2%
		Experiment	1.011		0.997		0.960		0.956		0.989	
	H/L=1/30	DIFFRACT	1.011	0.0%	0.999	0.2%	0.982	2.3%	0.984	2.9%	0.991	0.2%
		OpenFOAM	1.020	0.9%	0.970	-2.7%	0.937	-2.4%	0.958	0.2%	0.986	-0.3%
		Experiment	1.022		1.036		0.991		0.922		1.010	
T=15s	*H/L*=1/16	DIFFRACT	1.011	-1.1%	0.999	-3.6%	0.982	-0.9%	0.984	6.7%	0.991	-1.9%
		OpenFOAM	0.927	-9.3%	0.976	-5.8%	0.961	-3.0%	0.884	-4.1%	0.984	-2.6%
		Experiment	0.981		1.066		1.063		0.899		1.045	
	H/L=1/10	DIFFRACT	1.011	3.1%	0.999	-6.3%	0.982	-7.6%	0.984	9.5%	0.991	-5.2%
		OpenFOAM	0.929	-5.3%	0.944	-11.4%	0.937	-11.9%	0.791	-12.0%	0.908	-13.1%

Table 6 QTFs (2nd harmonics) of surface elevations at the inner circle of wave probes (see Table 1)

Wave probes			WPB1	Difference	WPB2	Difference	WPB3	Difference	WPB4	Difference	WPB5	Difference
		Experiment	0.474		0.207		1.084		0.956		0.872	
	H/L=1/30	DIFFRACT	0.613	29.3%	0.303	46.4%	1.097	1.2%	1.138	19.0%	1.200	37.6%
		OpenFOAM	0.683	44.1%	0.459	121.7%	1.087	0.3%	0.951	-0.5%	0.975	11.8%
		Experiment	0.556		0.360		0.942		0.685		0.886	
T=7s	*H/L*=1/16	DIFFRACT	0.613	10.3%	0.303	-15.8%	1.097	16.5%	1.138	66.1%	1.200	35.4%
		OpenFOAM	0.453	-18.5%	0.239	-33.6%	1.103	17.1%	0.611	-10.8%	0.763	-13.9%
		Experiment	0.755		0.609		0.957		0.539		0.724	
	H/L=1/10	DIFFRACT	0.613	-18.8%	0.303	-50.2%	1.097	14.6%	1.138	111.1%	1.200	65.7%
		OpenFOAM	0.471	-37.6%	0.420	-31.0%	0.699	-27.0%	0.454	-15.8%	0.543	-25.0%
		Experiment	0.559		0.186		0.698		0.369		0.449	
	H/L=1/30	DIFFRACT	0.659	17.9%	0.262	40.9%	0.814	16.6%	0.347	-6.0%	0.597	33.0%
		OpenFOAM	0.569	1.8%	0.338	81.7%	0.700	0.3%	0.282	-23.6%	0.467	4.0%
		Experiment	0.659		0.276		0.598		0.348		0.376	
T=9s	*H/L*=1/16	DIFFRACT	0.659	0.0%	0.262	-5.1%	0.814	36.1%	0.347	-0.3%	0.597	58.8%
		OpenFOAM	0.587	-10.9%	0.442	60.1%	0.606	1.3%	0.221	-36.5%	0.381	1.3%
		Experiment	0.500		0.369		0.466		0.290		0.336	
	H/L=1/10	DIFFRACT	0.659	31.8%	0.262	-29.0%	0.814	74.7%	0.347	19.7%	0.597	77.7%
		OpenFOAM	0.621	24.2%	0.511	38.5%	0.337	-27.7%	0.242	-16.6%	0.239	-28.9%
		Experiment	0.209		0.127		0.121		0.034		0.117	
	H/L=1/30	DIFFRACT	0.198	-5.3%	0.079	-37.8%	0.091	-24.8%	0.017	-50.0%	0.109	-6.8%
T=15s		OpenFOAM	0.216	3.3%	0.141	11.0%	0.146	20.7%	0.074	117.6%	0.083	-29.1%
		Experiment	0.253		0.181		0.040		0.045		0.106	
	H/L=1/16	DIFFRACT	0.198	-21.7%	0.079	-56.4%	0.091	127.5%	0.017	-62.2%	0.109	2.8%

		OpenFOAM	0.203	-19.8%	0.164	-9.4%	0.063	57.5%	0.056	24.4%	0.061	-42.5%
	H/L=1/10	Experiment	0.135		0.174		0.073		0.064		0.083	
		DIFFRACT	0.198	46.7%	0.079	-54.6%	0.091	24.7%	0.017	-73.4%	0.109	31.3%
		OpenFOAM	0.211	56.3%	0.193	10.9%	0.137	87.7%	0.065	1.6%	0.098	18.1%

Table 7 QTFs (2nd harmonics) of surface elevations at the outer circle of wave probes (see Table 1)

Wave probes			WPO1	Difference	WPO2	Difference	WPO3	Difference	WPO4	Difference	WPO5	Difference
T=7s	*H/L*=1/30	Experiment	0.330		0.193		0.666		1.142		0.950	
		DIFFRACT	0.263	-20.3%	0.237	22.8%	0.761	14.3%	1.298	13.7%	1.082	13.9%
		OpenFOAM	0.210	-36.4%	0.226	17.1%	0.639	-4.1%	1.113	-2.5%	0.960	1.1%
	H/L=1/16	Experiment	0.312		0.203		0.690		0.954		0.795	
		DIFFRACT	0.263	-15.7%	0.237	16.7%	0.761	10.3%	1.298	36.1%	1.082	36.1%
		OpenFOAM	0.350	12.2%	0.392	93.1%	0.585	-15.2%	0.812	-14.9%	0.818	2.9%
	H/L=1/10	Experiment	0.330		0.293		0.622		0.770		0.719	
		DIFFRACT	0.263	-20.3%	0.237	-19.1%	0.761	22.3%	1.298	68.6%	1.082	50.5%
		OpenFOAM	0.146	-55.8%	0.281	-4.1%	0.536	-13.8%	0.524	-31.9%	0.611	-15.0%
T=9s	*H/L*=1/30	Experiment	0.317		0.189		0.581		0.264		0.423	
		DIFFRACT	0.289	-8.8%	0.228	20.6%	0.686	18.1%	0.343	29.9%	0.582	37.6%
		OpenFOAM	0.349	10.1%	0.283	49.7%	0.603	3.8%	0.305	15.5%	0.450	6.4%
	H/L=1/16	Experiment	0.201		0.256		0.511		0.266		0.340	
		DIFFRACT	0.289	43.8%	0.228	-10.9%	0.686	34.2%	0.343	28.9%	0.582	71.2%
		OpenFOAM	0.186	-7.5%	0.174	-32.0%	0.517	1.2%	0.229	-13.9%	0.365	7.4%
	H/L=1/10	Experiment	0.108		0.134		0.386		0.245		0.314	
		DIFFRACT	0.289	167.6%	0.228	70.1%	0.686	77.7%	0.343	40.0%	0.582	85.4%
		OpenFOAM	0.080	-25.9%	0.129	-3.7%	0.386	0.0%	0.234	-4.5%	0.230	-26.8%
T=15s	*H/L*=1/30	Experiment	0.162		0.139		0.078		0.041		0.094	
		DIFFRACT	0.178	9.9%	0.117	-15.8%	0.033	-57.7%	0.042	2.4%	0.091	-3.2%
		OpenFOAM	0.171	5.6%	0.133	-4.3%	0.068	-12.8%	0.038	-7.3%	0.097	3.2%
	H/L=1/16	Experiment	0.193		0.164		0.100		0.030		0.097	
		DIFFRACT	0.178	-7.8%	0.117	-28.7%	0.033	-67.0%	0.042	40.0%	0.091	-6.2%
		OpenFOAM	0.126	-34.7%	0.119	-27.4%	0.073	-27.0%	0.008	-73.3%	0.070	-27.8%
	H/L=1/10	Experiment	0.170		0.130		0.122		0.075		0.115	
		DIFFRACT	0.178	4.7%	0.117	-10.0%	0.033	-73.0%	0.042	-44.0%	0.091	-20.9%
		OpenFOAM	0.099	-41.8%	0.086	-33.8%	0.107	-12.3%	0.091	21.3%	0.101	-12.2%

Table 8 RAOs (1st harmonics) and QTFs (2nd harmonics) of wave forces

Wave probes			$F_x^{(1)}/\rho g A r^2$	Difference	$F_z^{(1)}/\rho g A r^2$	Difference	$F_x^{(2)}/\rho g A^2 r$	Difference	$F_z^{(2)}/\rho g A^2 r$	Difference
T=7s	*H/L*=1/30	Experiment	5.583		0.401		0.461		0.259	
		DIFFRACT	4.940	-11.5%	0.266	-33.7%	0.348	-24.5%	0.422	62.9%
		OpenFOAM	5.077	-9.1%	0.279	-30.4%	0.546	18.4%	0.432	66.8%
	H/L=1/16	Experiment	5.069		0.384		0.380		0.230	
		DIFFRACT	4.940	-2.5%	0.266	-30.7%	0.348	-8.4%	0.422	83.5%
		OpenFOAM	4.761	-6.1%	0.296	-22.9%	0.566	48.9%	0.423	83.9%
	H/L=1/10	Experiment	5.146		0.407		0.329		0.262	
		DIFFRACT	4.940	-4.0%	0.266	-34.6%	0.348	5.8%	0.422	61.1%
		OpenFOAM	4.445	-13.6%	0.287	-29.5%	0.587	78.4%	0.365	39.3%
T=9s	*H/L*=1/30	Experiment	4.793		0.808		0.573		0.107	
		DIFFRACT	4.330	-9.7%	0.704	-12.9%	0.537	-6.3%	0.149	39.3%
		OpenFOAM	4.282	-10.7%	0.661	-18.2%	0.426	-25.7%	0.191	78.5%
	H/L=1/16	Experiment	4.473		0.814		0.511		0.087	
		DIFFRACT	4.330	-3.2%	0.704	-13.5%	0.537	5.1%	0.149	71.3%
		OpenFOAM	4.134	-7.6%	0.704	-13.5%	0.359	-29.7%	0.148	70.1%
	H/L=1/10	Experiment	4.249		0.901		0.434		0.084	

		DIFFRACT	4.330	1.9%	0.704	-21.9%	0.537	23.7%	0.149	77.4%
		OpenFOAM	3.818	-10.1%	0.715	-20.6%	0.259	-40.3%	0.162	92.9%
T=15s	*H/L*=1/30	Experiment	2.276		1.965		0.737		0.027	
		DIFFRACT	2.060	-9.5%	1.840	-6.4%	0.631	-14.4%	0.050	85.2%
		OpenFOAM	2.122	-6.8%	1.773	-9.8%	0.550	-25.4%	0.018	-33.3%
	H/L=1/16	Experiment	2.229		2.044		0.702		0.032	
		DIFFRACT	2.060	-7.6%	1.840	-10.0%	0.631	-10.1%	0.050	56.3%
		OpenFOAM	1.980	-11.2%	1.808	-11.5%	0.421	-40.0%	0.030	-6.3%
	H/L=1/10	Experiment	2.198		2.188		0.598		0.038	
		DIFFRACT	2.060	-6.3%	1.840	-15.9%	0.631	5.5%	0.050	31.6%
		OpenFOAM	1.877	-14.6%	1.753	-19.9%	0.468	-21.7%	0.056	47.4%